Journal of Electromagnetic Waves and Applications

ISSN: (Print) (Online) Journal homepage: www.tandfonline.com/journals/tewa20

High-precision reading of a weak magnetostatic field

H. Citak

To cite this article: H. Citak (2024) High-precision reading of a weak magnetostatic field, Journal of Electromagnetic Waves and Applications, 38:9, 1026-1040, DOI: 10.1080/09205071.2024.2354717

To link to this article: https://doi.org/10.1080/09205071.2024.2354717

Published online: 21 May 2024.

JOURNAL OF ELECTROMAGNETIC WAVES AND APPLICATIONS
2024, VOL. 38, NO. 9, 1026–1040
https://doi.org/10.1080/09205071.2024.2354717

High-precision reading of a weak magnetostatic field

H. Citak

Department of Electricity and Energy, Balikesir Vocational School of Higher Education, Balikesir University, Balikesir, Turkey

ABSTRACT

Efforts have recently been put into developing proton precession magnetometers (PPM) in order to measure weak magnetic fields with high precision. Although high-cost commercial PPMs are available today, there are ongoing studies for low power consumption, low cost, high accuracy and resolution. Accordingly, in this study, a new PPM with a measurement range of 20,000 nT-120,000 nT, a production cost of $2000 and an accuracy of 0.13 nT was developed and its performance in determining the earth's magnetic field was examined. It was determined that the developed PPM has an advantage over its commercial equivalents (G857, WCZ, etc.) in terms of price-performance ratio and can be used to determine small magnetic field values such as the earth's magnetic field.

ARTICLE HISTORY
Received 22 September 2023
Accepted 8 May 2024

KEYWORDS
Magnetic sensors; proton magnetometer; SNR ratio; FFT analysis; FID signal

PACS NOS
91.25.-r; 32.10.Dk; 87.50.C-; 07.55.Ge; 07.55.Jg

1. Introduction

Currently, many magnetic sensors exist that are based on Hall and magneto-resistive effect. In a Hall sensor, the magnitude of the magnetic field is determined by the magnitude of the Hall voltage, whereas in MR sensors (AMR, GMR, TMR, etc.), the angle between the direction and magnitude of the magnetization induced by the magnetic field and the direction of the current flowing through the MR sensor greatly affects output voltage [1–8]. When one intends to measure weak static or dynamic magnetic fields using such sensors, electromagnetic noise becomes dominant, which reduces signal-to-noise ratio (SNR) and measurement accuracy. Therefore, proton precession magnetometers (PPM) are preferred for measuring weak magnetic fields with high precision.

Weak magnetic field measurement is widely used in many areas such as space research, national defense, geology and mineral resources research and medical devices [9,10]. PPM has still been the most widely-used geomagnetic research tool since half a century, thanks to its superior stability and ease of use [11,12]. There are many commercial products currently available in the market, such as WCZ series produced by Chongqing University, Southwest Jiaotong University, Geophysical Team of Yellow River Comittee, and being a member of Chinese Society of Geology, BTSK/LANGEO, G856 and GSM-19 T produced by GEM company of Canada, etc. On the other hand, most of such PPMs have low

CONTACT H. Citak hcitak@balikesir.edu.tr Department of Electricity and Energy, Balikesir Vocational School of Higher Education, Balikesir University, Balikesir, 10145, Turkey

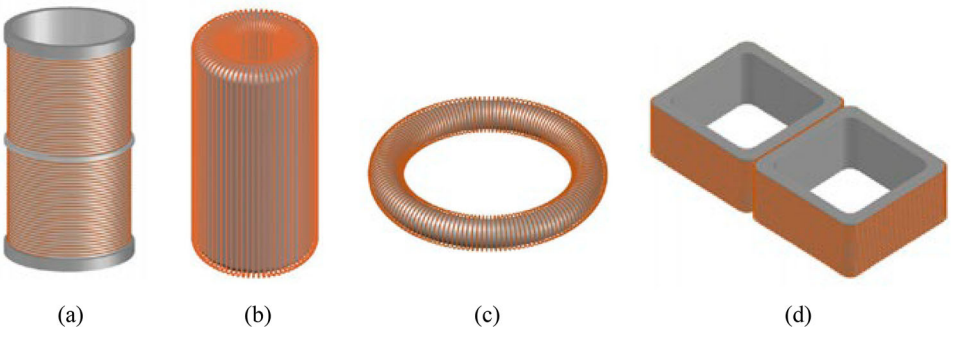

Figure 1. Different coil structures used in the production of proton magnetometers.

resolution and are easily affected by external magnetic media [13,14]. Therefore, the development of PPM with higher accuracy and precision has attracted the attention of many researchers [15,16].

PPM basically consists of a solution and a coil. Solution types mostly contain deionized water, paraffin oil, methanol, alcohol, glycerin, etc. It is desirable that the solution has as many hydrogen protons as possible. The amount of protons in the solution affects the signal distortion time and the initial amplitude of the measurement signal. There are 4 different types of coils used in the production of proton magnetometers. These are 8 types of coils [17], solenoid, toroidal and cylindrical coils [18] (Figure 1).

For measuring the magnetic field, PPM utilizes the Larmor precession effect of the excited proton system [19]. Protons continuously rotate around their centers and therefore have angular momentum and magnetic moment according to atomic physics. Nevertheless, in the absence of a magnetic field in the surrounding environment, the magnetic moments of all the protons in the solution become irregular, resulting in a total magnetic moment of zero. Once the magnetometer is positioned within a stationary magnetic field for measurement, the total magnetic moment of the protons in the solution aligns in parallel with the direction of the static magnetic field. In this situation, there is no Larmor precession effect. A polarization current of short duration needs to be applied to the coil of the magnetometer in order to create the Larmor precession effect. The polarization current generated will create a polarization magnetic field (B_0) perpendicular to the magnetic field to be measured. The magnetic moments of the protons in the solution will be directed towards the direction of the resultant of the polarizing magnetic field and the magnetic field to be measured. The greater the polarizing magnetic field, the closer the angle between the magnetic field to be measured and the total magnetic field will be to 90 degrees. Cutting off the polarization current results in the polarized proton magnetic moments performing a Larmor precession along the direction of the magnetic field being measured (Figure 2) [20].

The precession frequency of the FID signal (ω_0) is directly related to the external magnetic field (B_0), as given in Equation (1). As shown in Equation (2), the proton magnetization (M_0) directly influences the magnitude of the FID signal (ϵ).

$$\omega_0 = \gamma_p . B_0 \tag{1}$$

$$\varepsilon \propto M_0 = N.\mu.\tan h.\left(\frac{\mu.B_0}{k.T}\right) \tag{2}$$

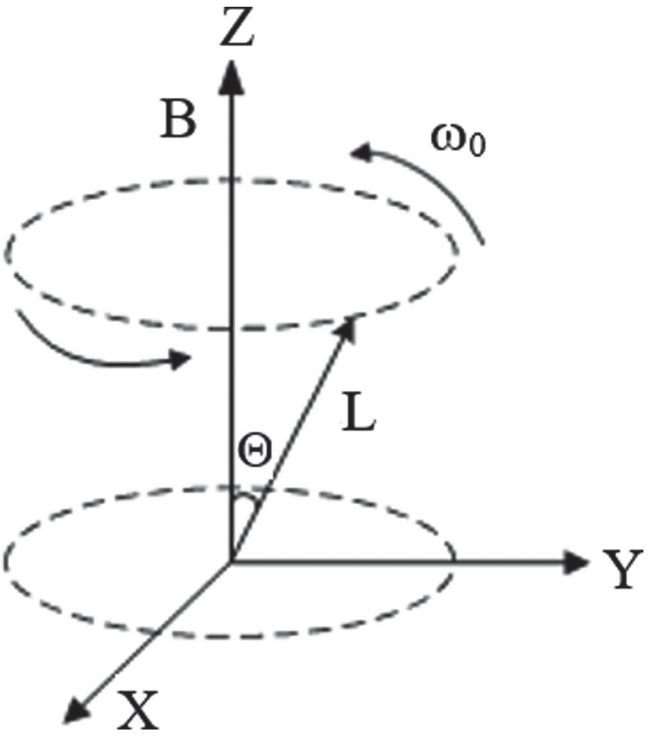

Figure 2. Larmor precession of the proton.

where N, μ, T and k are the number of protons in solution, a single proton's magnetic moment, the temperature in Kelvin and the Boltzmann constant, respectively. The amplitude of the FID signal induced in the magnetometer coil can be calculated using Equation (3) [21].

$$\varepsilon(t) = \varepsilon_0 e^{-t/T_2}.\cos\omega_0 t \tag{3}$$

where ϵ_0 represents the initial amplitude ($\mu_0.n.\text{A.M}.\omega_0$), T_2 represents the transverse relaxation time. The magnetometer's accuracy is defined by the SNR of the signal and the performance of the frequency measurement algorithm. The signal's SNR is determined by the sample and the pickup coil. Generally, a proton-rich and easy-to-polarize solution with a long T_2 is selected as the sample, such as paraffin oil. In PPM, there are three conventional coil structures to collect signals: Solenoidal, Cylindrical and Toroidal coils. When compared to other structures, solenoidal coils have a regular shape that is easy to design and manufacture, and are commonly used as sensing or polarization coils. Magnetic field distribution is nearly uniform at the center of the coil, thus providing favorable conditions for the PPM sample's uniform polarization. The amplitude of the signal induced in the solenoid due to the precessional motion can be calculated using Equation (4) [21].

$$e(t) \cong \frac{\chi.\omega.\mu_0.n^2.I}{\sqrt{2}.b^2}\upsilon.\sin\alpha \tag{4}$$

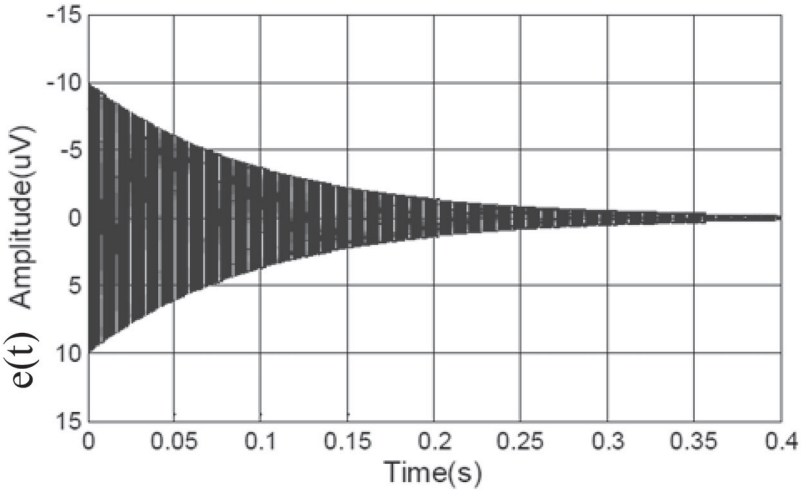

Figure 3. Change of (t) in a proton magnetometer (FID Signal).

where χ is the protons' nuclear paramagnetic susceptibility in the sample, ω is the proton's precession frequency in geomagnetics, e is the voltage of the signal. n, b, v, I and α define the number of turns, length of the solenoid, volume, polarization current, the angle between the area to be measured and the axis of a solenoid, respectively. When a Proton magnetometer operates, a sine wave (FID) is obtained, which has an exponentially decreasing magnitude and an amplitude at μV level (Figure 3). Precession of the protons causes the sinusoidal signal induced in the coil to decrease exponentially, as it is affected by thermal collisions. In addition to SNR, the relaxation constant of the signal is also related to the number of protons in the solution used.

The (t) amplitude being large results in a high SNR, which allows electromagnetic noise to be neglected in magnetic field measurement. SNR for a solenoidal coil can be calculated using Equation (5) [22].

$$\begin{aligned} SNR &= \eta_{single} \frac{\chi.\omega_L.\mu_0.\eta_m.\sqrt{n}.E.\pi.r_c^2.r_w^3.\sin\alpha}{2b[(r_c + r_w.l_s).\rho]^{3/2}\sqrt{19{,}2.k.T}} \\ \eta_{single} &= \exp(-1, 4r_c/2b) \\ \eta_m &= \exp(-1, 4r_c/b) \end{aligned} \tag{5}$$

where χ, μ_0, E and ω_L are the nuclear paramagnetic susceptibility of the proton-rich material, the magnetic permeability of the vacuum, the voltage of the polarization source and the proton precession signal's Larmor precession angular frequency, respectively. α is the angle between the local geomagnetic field and the axis of the sensor, T is the temperature, k is the Boltzmann constant, and η_m (filling factor) describes the inequality of the polarization field along the entire cross-section of the sensor.

When SNR is large and electromagnetic noise is not taken into consideration, (t) variation is determined by the performance of the frequency measurement algorithm used and the accuracy of the Larmor precession frequency. Equation (6) represents the relation

Table 1. Comparisons of commercial proton precession magnetometers.

Commercial Products	Resolution	Accuracy	Measuring Range	Price
G-857 [24]	0.1nT	0.5nT	20,000nT ~ 90,000nT	$5000
WCZ-1 [25]	0.1nT	1nT	20,000nT ~ 100,000nT	$5200
WCZ-1B [25]	0.1/0.05nT	0.5/1nT	20,000nT ~ 100,000nT	$7000
WCZ-3 [25]	0.05nT	0.5nT	20,000 nT ~ 100,000nT	$12,000
GSM-19 T [26,27]	0.01nT	0.2nT	20,000nT ~ 120,000nT	$12,500

between the Larmor precession frequency and the magnetic field to be measured [23].

$$B_0(nT) = 23,4874.f_p(Hz) \tag{6}$$

Moreover, the performance of the proton magnetometer is related to the relaxation constant of the signal and the initial amplitude of the FID signal. The higher the initial amplitude of the signal, the higher the relaxation time and the signal-to-noise ratio of the proton magnetometer, and hence the longer the effective measurement time.

The magnitude of the magnetic field is determined through a frequency analysis of the FID signal. Although high-cost commercial proton magnetometers are available today, there are ongoing studies for low cost, high accuracy and high resolution (Table 1).

Therefore, in this study, a new proton magnetometer was developed and its performance in determining the earth's magnetic field was investigated. In order to improve the sensitivity of the developed PPM, it was focused on the SNR value and the amplitude of the FID signal. Proton-rich paraffin was preferred to increase the amplitude of the FID signal. Thus, it was aimed to increase the SNR signal and attenuation constant. In addition, the development of a LabVIEW-based software for recording the FID signal to the computer with a high sampling rate and real-time FFT analysis and high-precision frequency measurement makes the study important. Therefore, the developed PPM is advantageous in terms of price-performance ratio compared to its commercial equivalents.

2. Structure of the developed proton precession magnetometer

The block structure of the PPM system developed within the scope of the study is demonstrated in Figure 4. The developed system can be analyzed under two main sections: software and hardware. In the first phase of the study, the hardware part of the system was completed and then the LabVIEW-based software part was written.

The hardware used in the PPM system consists of a sensor, a computer, an NI 6210 DAQ board, a preamplifier circuit, a narrowband filter circuit and a high-precision monolithic instrumentation amplifier circuit designed for data collection applications that require high accuracy. The developed PPM system is given in the Appendix.

2.1. Sensor

In this study, a solenoid coil was preferred for the sensor. However, a single solenoid coil has low capability to decrease external electromagnetic noise. Considering the fact that the PPM system will generally be used in environments with complex electromagnetic noise (noise from devices operating at 50/60 Hz) and the precession signal will be so weak (μV level), two reverse-wound serial coils were used instead of a single solenoid coil.

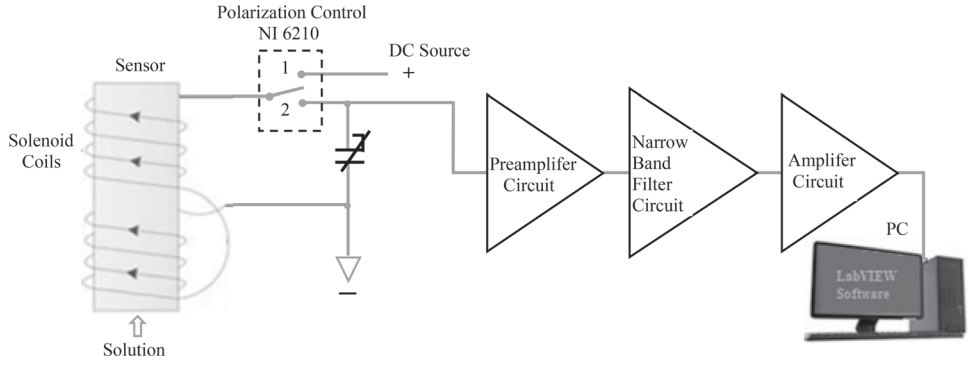

Figure 4. Block diagram of the developed PPM system.

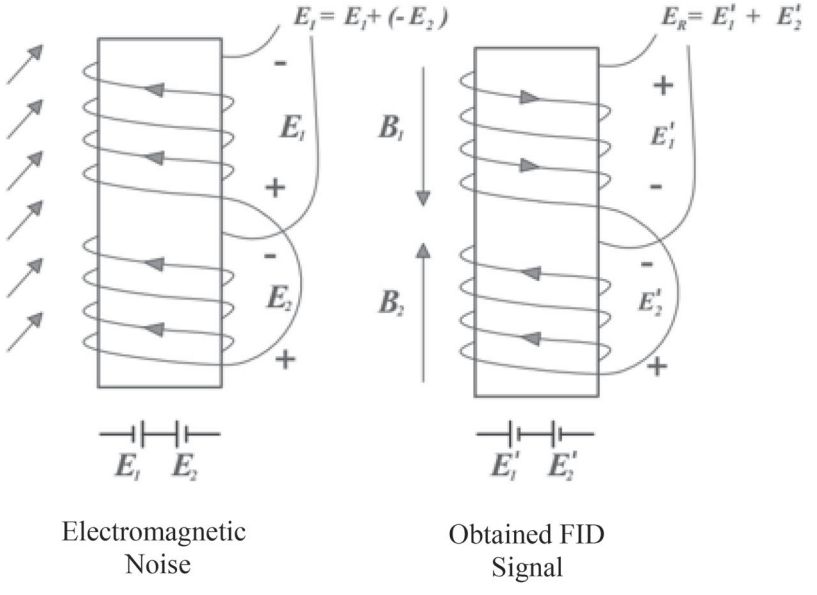

Figure 5. Noise-canceling design of the sensor.

Thus, the frequency shift caused by the capacitance of the coil was reduced and external electromagnetic noise was avoided.

As shown in Figure 5, if the inductance of both coils is equal, the magnitudes of the electromotor force induced in the coils due to external electromagnetic noise will be the same. The total effect (E_I) will be zero (Equation (7)).

$$E_I = E_1 + (-E_2) = 0 \tag{7}$$

Since the two coils are connected in series and reversed, the direction of the polarization magnetic field generated in the coils will be opposite to each other when the Larmor signal (E_R) is received. In this case, the electromotor force induced in the coils E_1' and E_2' are in

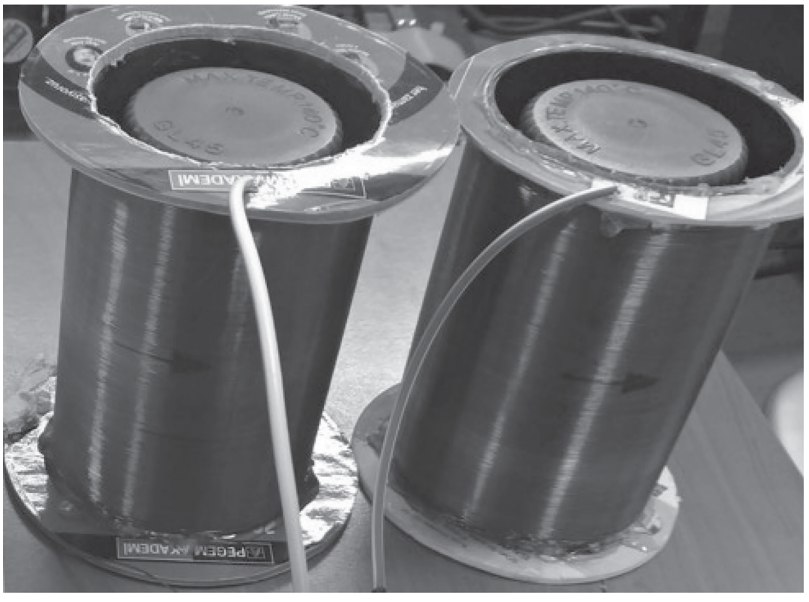

Figure 6. Two reverse-wound serial coils.

Table 2. Specifications of the coils.

Parameters	Values
Wire type	SWG19
Coil length	0.078 m
Diameter of the solution container	0.058 m
Number of coil windings	660
Number of layers	5
DC resistance	16.9 Ω
Inductance	31.681 mH
Polarization current (for 12 V)	0.656 A
Maximum allowed current	1 A
Filling factor	0.594
RMS Signal amplitude	0.9 μV
SNR (for 400 Hz bandwidth)	61 dB
Setting (resonance) capacitor (for 2000 Hz precession frequency)	150.25 nF

the same direction and can be found by Equation (8).

$$\mathrm{E}_R = E_1' + E_2' = 2E_1' = 2E_2' \tag{8}$$

The structural parameters of both coils should be as similar as possible. In this way, the coil set will not be affected by external disturbances, and the induction of the FID signal will not change due to this reason. In this study, all parameters for the two reverse-wound serial coils used for a noise-free FID signal were assumed to be the same, the values of which are provided in Table 2 (Figure 6).

Liquid paraffin was preferred in this study as the solution for the sensor due to its high number of protons. This aimed to increase SNR and the relaxation constant.

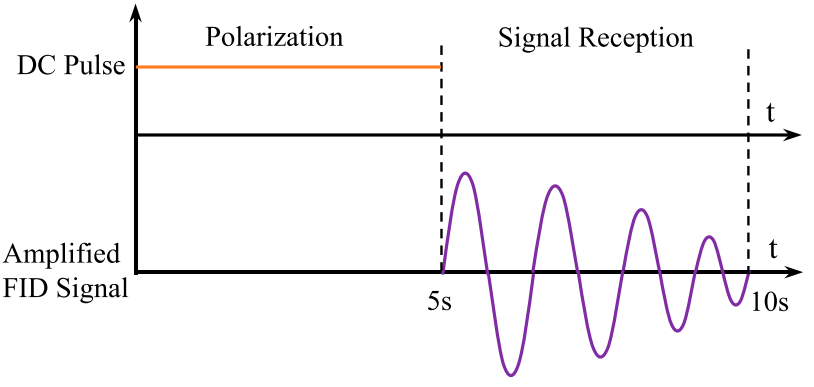

Figure 7. FID signal captured into the computer.

2.2. NI 6210 DAQ board

An NI6210 data capture card with 16 AI (16 bit, 256 kS/s) and 4 DIO was used in the study for both controlling the polarization current and capturing the amplified FID signal into the computer. The amplified and filtered FID signal was connected to the analog input of the DAQ card and recorded to the computer with 16-bit resolution and 250 kS/s sampling rate. The frequency value determined after FFT analysis of the recorded FID signal was converted into magnetic field magnitude by using Equation (6).

2.3. Resonance (setting) capacitor selection

The amplitude of the FID signal obtained following interruption of the polarization current is desired to be the greatest. Therefore, a resonance capacitor in parallel to the coil should be used after switching. The value of this capacitor depends on the magnitude of the magnetic field to be measured or the frequency of the FID signal. Since the study aims to measure the magnetic field of the earth at our location (46,000 nT, FID frequency 2000 Hz), the capacitance value was calculated as 150.25 nF by using Equation (8) below.

$$C_r = \frac{1}{4.\pi^2.f_p^2.L} \tag{9}$$

2.4. Preamplification, narrow band filter and monolithic instrumentation amplifier circuits

Although the resonance state is achieved, the FID signal obtained from the sensor has an amplitude at μV levels. Therefore, it needs to be amplified before the narrow band filter. In this study, the preamplification coefficient was determined as $10*10 = 100$. The FID that is gradually amplified 100 times was subsequently fed into a narrowband filter with a bandwidth of 400 Hz, which allows frequencies between 1800 and 2200 Hz to pass through. Finally, the filter output was amplified 1000 times using a precision amplifier circuit utilizing an AD524 integrated circuit, and captured into the computer via the NI6210 DAQ board (Figure 7).

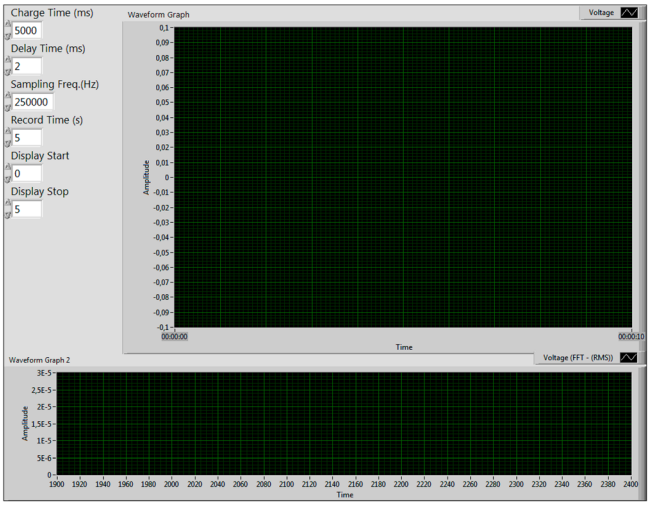

(a)

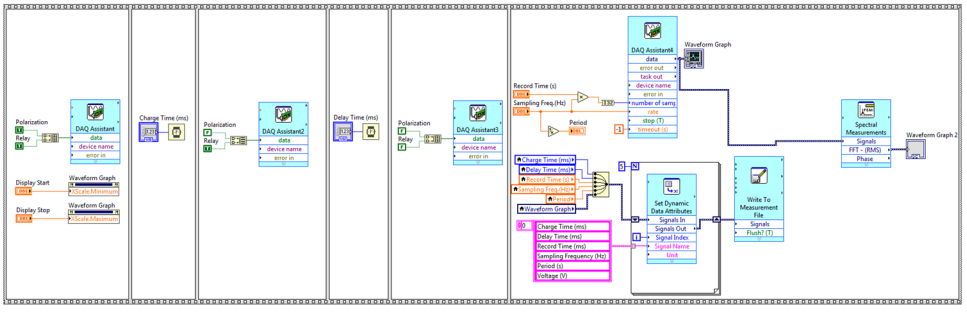

(b)

Figure 8. (a) Front Panel and (b) Block Diagram of the developed LabVIEW-based software.

2.5. The LabVIEW-based software

The developed LabVIEW-based software controls the application time of the polarization current and records the FID signal amplified 2 ms after switching into the computer medium for a period of 5 s. It subsequently performs an FFT analysis of the recorded FID signal. The Front Panel and the Block Diagram of the developed software are demonstrated in Figure 8.

3. An application for the developed PPM system

In order to test the usability of the PPM system developed within the scope of this study, we made an attempt to calculate the magnetic field of the earth at our location. As is known, the magnitude and direction of the earth's magnetic field vary according to time. Therefore, the World Magnetic Model (WMM) platform, a joint product of the United Kingdom Defense Geographic Center (DGC) and the United States National Geospatial-Intelligence Agency (NGA), was used as a reference for the magnitude of the magnetic field at our location. The

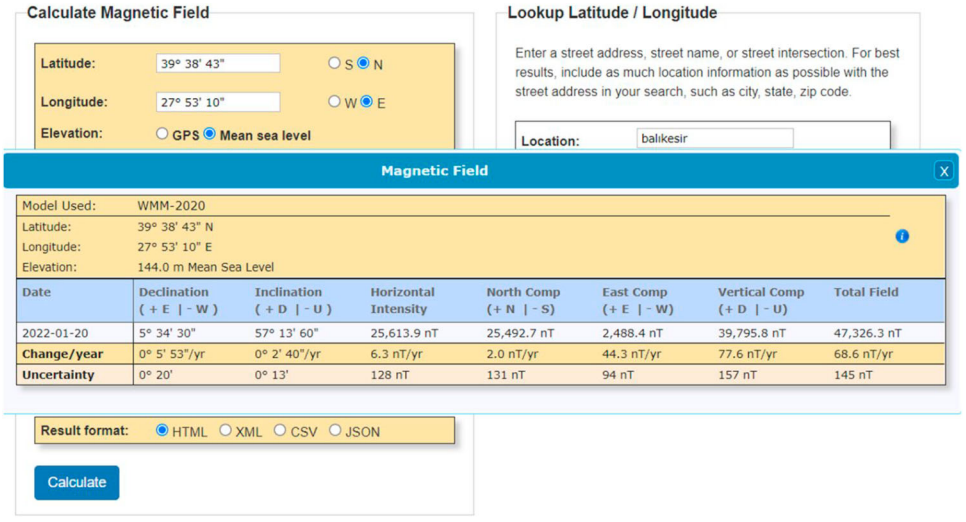

Figure 9. WMM Platform output for Balikesir.

direction and magnitude of the magnetic field calculated for Balikesir/Turkey according to this platform are demonstrated in Figure 9.

As seen in Figure 9, the total magnetic field magnitude in Balikesir is 47.326 nT. This corresponds to an FID signal of approximately 2004 Hz, according to Equation (6). In our study, the sensor of the PPM system developed to obtain this value was directed to the appropriate angle and a measurement was made. The output of the PPM system is shown in Figure 10.

As can be seen in Figure 10(b), the maximum FFT component is 2003.5 Hz. When calculated by considering Equation (6), the magnetic field value is obtained as 47,057 nT. Figure 10 also shows that both the measurement of the PPM system and the output of the WWM platform are close and that the system eliminates electromagnetic noise well. In addition, the value measured by the developed PPM was also verified with a tesla meter from F.W.BELL (Model 5180). The values of SNR parameters are given in Table 3. As a result of the calculation using the SNR parameters given in Table 3 in Equation (5), this ratio was found as 61 dB.

In addition, the accuracy of the developed PPM system depends on the accuracy of the self-induction coefficient of the resonance capacitor and coils used in the electronics of the system. These values are 0.005 nF and 0.0005 mH for the developed system, respectively. In the study, the accuracy of the system was calculated with Equation (10) considering these values and it was found as 0.13 nT.

$$\Delta B = 23.4874\left[\frac{1}{4.\pi.C^{1/2}.L^{3/2}}\Delta L + \frac{1}{4.\pi.C^{3/2}.L^{1/2}}\Delta C\right] \tag{10}$$

4. Discussion

PPMs can often be more complex and costly than other magnetic sensors. The cost of the system in this study is significantly lower than other commercial equivalents. Therefore,

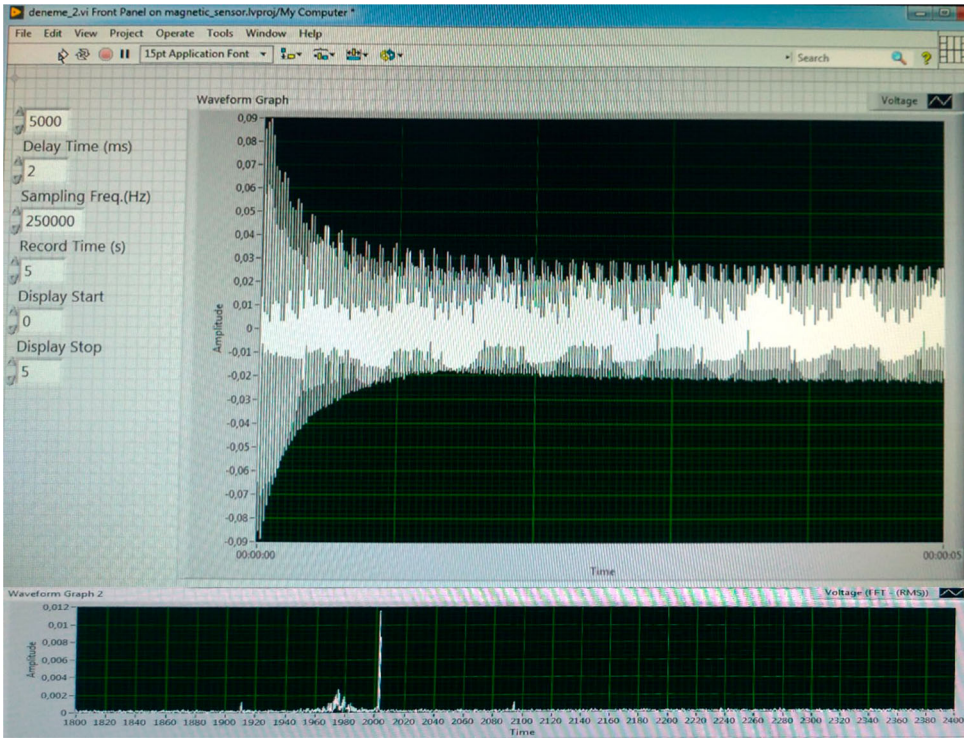

Figure 10. FID signal variation, and FFT analysis output for the measurement of the earth's magnetic field using the developed PPM system.

Table 3. SNR parameters.

Parameters	Values
Fill Factor of a Coil (η_{single})	$7.71\ 10^{-1}$
Nuclear Paramagnetic Susceptibility (χ)	$9.1\ 10^{-6}$
Larmor Precession angular Frequency (ω_L)	$1.78\ 10^{3}$ rad/s
Magnetic Permeability of the Vacuum (μ_0)	$1.26\ 10^{-6}$ T.m/A
Filling Factor (η_m)	$5.94\ 10^{-1}$
Number of Turns (n)	660
Voltage of Polarization Source (E)	12 V
Radius of Winding (r_c)	$2.9\ 10^{-2}$ m
Angle Between the Measured Area and the Axis of Solenoid (α)	0.9°
Radius of Wire (r_w)	$3.05\ 10^{-4}$ m
Length of Solenoid (b)	$7.8\ 10^{-2}$ m
Layer of Winding (l_s)	5
Wire Resistivity (ρ)	$6.89\ 10^{-8}$ Ωm
Boltzmann Constant	$1.38\ 10^{-23}$ J/K
Environmental Temperature (T)	$3\ 10^{2}$ K

the choice of PPM should be based on application needs and factors such as sensitivity requirement, measurement range, environment and budget.

In addition to coil configuration, one of the important indicators for evaluating the performance of PPM sensors is SNR. In PPM applications, SNR is usually between 20 and 40 dB [18,19,28,29], but it should be noted that higher SNR values may be needed, especially in sensitive applications where low magnetic field levels are measured. Therefore, the

Table 4. Comparison of commercial and developed PPMs.

Model	Resolution	Accuracy	Measuring range	Price
Commercial Products	0.072nT	0.59nT	20,000nT ~ 102,000nT	$8340
Developed PPM	0.2nT	0.13nT	20,000nT ~ 120,000nT	$2000

SNR value of 61 dB in this study will help to obtain more reliable and accurate magnetic field measurements. A comparison of the features of the developed PPM system with its commercial equivalents is given in Table 4.

5. Conclusion

In this study, a novel PPM system was developed and its measurement accuracy was verified through an example application. Liquid paraffin was used as a solution in the sensor of the system, which distinguishes the study from others in the literature. SNR is an important indicator for evaluating the performance of a PPM system. The SNR of the developed PPM system is significantly higher than its counterparts available in the market. However, the type of coil used in the developed PPM system has a dead measurement point. Therefore, the sensor probe should always be kept perpendicular to the magnetic field to be measured, to the extent possible, in order to obtain maximum FID signal amplitude. It is also crucial for the aforesaid type of magnetic sensors that thermal noise and external electromagnetic noise of the sensor are minimized. Reverse-wound series coils were used in this study in order to cancel out electromagnetic noise. In order to eliminate sensor-induced thermal noise, the resistance of the coil has been reduced. The resistance of a magnetic coreless solenoidal coil such as the one in this study was determined by Equation (11) using the parameters of the coil structure, namely coil hollow radius r, winding thickness h, wire resistivity ρ, winding diameter d and coil volume V. In the study, d was increased for the purpose of obtaining coils with low R resistance.

$$R = \frac{16.\rho.V.h}{\pi.d^2(2r+h)} \tag{11}$$

The most important issue in the developed PPM system is the lossless high-speed acquisition and evaluation of the FID signal. This depends on the response time of the system's electronics, data acquisition card and software. Although there is no speed problem in this system due to the data acquisition card and software, it may be preferable that the integrated circuits in the amplification and filter circuits have faster response times. However, although this increases the cost, it may contribute to more accurate determination of the maximum FID signal. Future work will focus on a mobilized system designed with integrated circuits with lower response times.

Disclosure statement

No potential conflict of interest was reported by the author(s).

Data availability statement

Data sharing does not apply to this article as no datasets were generated or analyzed during the current study.

Notes on contributors

Hakan Citak was born in Romanshorn, Switzerland in 1969. He received the B.S. and Ph.D. degrees from the Department of Electric Education, Institute of Science, Marmara University, Istanbul, Turkey, in 1995 and 2014, respectively. He is currently working for the Balikesir Vocational High School, Electric Program, Balikesir University, Balikesir. His research interests are magnetic sensors and magnetic anomaly. He holds two patents.

References

[1] Venikar PA, Ballal MS, Umre BS, et al. Search coil based online diagnostics of transformer internal faults. IEEE Trans Power Deliv. 2017;32(6):2520–2529. doi:10.1109/TPWRD.2017.2682083
[2] Liu S, Sun Y, Jiang X, et al. Comparison and analysis of multiple signal processing methods in steel wire rope defect detection by Hall sensor. Measurement. 2021;171:1–20. doi:10.1016/j.measurement.2020.108768.
[3] Nazlıbilek S, Kalender O, Ege Y. Mine identification and classification by mobile sensor network using magnetic anomaly. IEEE Trans Instrum Meas. 2011;60(3):1028–1036. doi:10.1109/TIM.2010.2060220
[4] Ege Y, Şensoy MG, Kalender O, et al. Numerical analysis for remote identification of materials with magnetic characteristics. IEEE Trans Instrum Meas. 2011;60(9):3140–3152. doi:10.1109/TIM.2011.2124651
[5] Ege Y, Nazlibilek S, Kakilli A, et al. A Study on the performance of magnetic material identification system by SIFT–BRISK and neural network methods. IEEE Trans Magn. 2015;51(8):1–16. doi:10.1109/TMAG.2015.2408572.
[6] Ege Y, Çoramık M, Kabadayı M, et al. Anomaly detection with low magnetic flux: a fluxgate sensor network application. Measurement. 2016;81:43–56. doi:10.1016/j.measurement.2015.12.004
[7] Ege Y, Coramik M. A new measurement system using magnetic flux leakage method in pipeline inspection. Measurement. 2018;123:163–174. doi:10.1016/j.measurement.2018.03.064
[8] Gunes H, Bicakcı S, Citak H, et al. Buried magnetic material detection system: an SVM algorithm application. IEEE Trans Magn. 2021;57(7):1–9. doi:10.1109/TMAG.2021.3077864.
[9] Winslow RM, Johnson CL, Anderson BJ, et al. Observations of mercury's northern cusp region with MESSENGER's magnetometer. Geophys Res Lett. 2012;39(8):1–6. doi:10.1029/2012GL051472.
[10] Liu H, Dong H, Liu Z, et al. A comprehensive study on the weak magnetic sensor character of different geometries for proton precession magnetometer. J Instrum. 2018;13(9):1–18. doi: 10.1088/1748-0221/13/09/T09003.
[11] Dong H, Changda Z. A further review of the quantum magnetometers. Chin J Eng Geophys. 2010;7(4):461–470.
[12] Chao T, Dong H, Ge Z. OVERHAUSER magnetometer excitation and receiving system design. Chin J Sci Instrum. 2010;31(8):1867–1872.
[13] Denisov AY, Sapunov VA, Rubinstein B. Broadband mode in proton-precession magnetometers with signal processing regression methods. Meas Sci Technol. 2014;25(5):1–6. doi:10.1088/0957-0233/25/5/055103.
[14] Liang SQ, Yang GQ, Xu YF, et al. Simultaneously improving the sensitivity and absolute accuracy of CPT magnetometer. Opt Express. 2014;22(6):6837–6843. doi:10.1364/OE.22.006837
[15] Zhang S, Zhou Q, Chen S, et al. Design of JPM-1 proton magnetometer based on DSP. J Jilin Univ (Information Science Edition). 2014;32(5):509–515.
[16] Xiao X, Xiaofei Y, Ouyang J. Researching of applying magnetic tensor in range finding magnetic sub-stance. Electron Meas Technol. 2013;4:15–19.
[17] Mahavarkar P, Singh S, Labde S, et al. The low cost proton precession magnetometer developed at the Indian institute of geomagnetism. J Instrum. 2017;12(5):1–10. doi:10.1088/1748-0221/12/05/T05002.

[18] Liu H, Liu H, Dong H, et al. Noise characterization for the FID signal from proton precession magnetometer. J Instrum. 2017;12(7):1–14. doi:10.1088/1748-0221/12/07/P07019.
[19] Liu H, Dong H, Ge J, et al. A high precision proton magnetometer based on a multi-channel frequency measurement. 2016 IEEE International Instrumentation and Measurement Technology Conference Proceedings; 2016 May 23–26; Taipei, Taiwan. doi:10.1109/I2MTC.2016.7520474
[20] Zhang Y, Shudong C, Shuang Z. Study on methods of sensitivity evaluation of JPM-4 proton magnetometer. IOP Conference Series: Materials Science and Engineering. 2019;563(2):1–6. doi:10.1088/1757-899X/563/2/022028.
[21] Luo W, Dong H, Ge J, et al. Research on an omnidirectional proton precession magnetometer sensor based on solenoidal coils. 2019 IEEE International Instrumentation and Measurement Technology Conference (I2MTC); 2019 September 9; Auckland, New Zealand. doi:10.1109/I2MTC.2019.8827001
[22] Ruhunusiri WDS, Jayananda MK. Construction of a proton magnetometer. Proceedings of the Technical Sessions; 24; 2008; Sri Lanka. p. 78–85.
[23] Ping X, Shuang Z, Shudong C. The analysis of the polarization circuit to Proton precession magnetometer. 2012 International Conference on Industrial Control and Electronics Engineering; 2012 August 23–25; Xi'an, People's Republic of China. doi:10.1109/ICICEE.2012.140
[24] Available from: https://www.geometrics.com/product/g-857/ [cited 14.02.2024]
[25] Available from: http://www.langeoinstrument.com/Digital_Proton_Magnetometer/ [cited 14.02.2024]
[26] Available from: https://www.gemsys.ca/versatile-proton-magnetometer-gradiometer/ [cited 14.02.2024]
[27] Ma N, Chen S, Zhang S. Proton magnetometer sensor design and its performance. 3rd International Forum on Geoscience and Oceanography. IOP Conf. Series: Earth and Environmental Science; 2021 March 12–14; Suzhou, People's Republic of China. doi:10.1088/1755-1315/734/1/012028
[28] Gong X, Chen S, Zhang S, et al. JPM-4 Proton Precession Magnetometer and sensitivity estimation. Sens Mater. 2022;34(1):13–26. doi:10.18494/SAM3719
[29] Mahboubian F, Sardari H, Sadeghi S, et al. Design and implementation of a low noise earth field proton precession magnetometer. 27th Iranian Conference on Electrical Engineering; 30 April–02 May 2019; Yazd, Iran. p. 345–347.

Appendix


PC Connection
Solution
Solution
Electronic Card
NATIONAL INSTRUMENTS
Coil 1
Coil 2
DAQ Card
Power Supply